Stratigraphic context and age of hominin fossils from Middle Pleistocene Flores

Adam Brumm[1,2]*, Gerrit D. van den Bergh[3]*[#], Michael Storey[4], Iwan Kurniawan[5]*, , Brent V. Alloway[6,3], Ruly Setiawan[7,3], Erick Setiyabudi[5], Rainer Grün[8,1], Mark W. Moore[9], Dida Yurnaldi[7,3], Mika R. Puspaningrum[3], Unggul P. Wibowo[5,3], Halmi Insani[5], Indra Sutisna[5], John A. Westgate[10], Nick J.G. Pearce[11], Mathieu Duval[12], Hanneke J.M. Meijer[13], Fachroel Aziz[5], Thomas Sutikna[3,14], Sander van der Kaars[15,16], Michael J. Morwood[3§]

Author affiliations

[1]Research Centre of Human Evolution, Environmental Futures Research Institute, Griffith University, Nathan QLD 4111, Australia.

[2]School of Earth & Environmental Sciences, University of Wollongong, Wollongong NSW 2522, Australia.

[3]Centre for Archaeological Science, School of Earth & Environmental Sciences, University of Wollongong, Wollongong NSW 2522, Australia.

[4]Quadlab, Natural History Museum of Denmark, University of Copenhagen, 12 DK-1350 Copenhagen, Denmark.

[5]Geology Museum, Bandung 40122, Indonesia.

[6]School of Geography, Environment and Earth Sciences, Victoria University, Wellington 6012, New Zealand.

[7]Center for Geological Survey, Geological Agency, Bandung 40122, Indonesia.

[8]Research School of Earth Sciences, The Australian National University, Canberra ACT 2601, Australia.

[9]Stone Tools and Cognition International Research Hub, School of Humanities,

University of New England, Armidale NSW 2351, Australia.

[10]Department of Earth Sciences, University of Toronto, Toronto, Ontario M5S 3B1, Canada.

[11]Department of Geography & Earth Sciences, Aberystwyth University, Wales SY23 3DB, United Kingdom.

[12]Geochronology, Centro Nacional de Investigación sobre la Evolución Humana (CENIEH), Paseo de Atapuerca, 3, 09002-Burgos, Spain.

[13]University Museum of Bergen, University of Bergen, 5007 Bergen, Norway.

[14]National Research Centre for Archaeology (ARKENAS), Jakarta 12510, Indonesia.

[15]Cluster Earth & Climate, Faculty of Earth and Life Sciences, Vrije Universiteit, HV 1081 HV Amsterdam, the Netherlands.

[16]School of Earth, Atmosphere and Environment, Monash University, Clayton VIC 3800, Australia.

[§]Deceased

**These authors contributed equally*

[#]Correspondence and requests for information should be addressed to G.D.v.d.B. (gert@uow.edu.au)

Recent excavations at the early Middle Pleistocene site of Mata Menge in the So'a Basin of central Flores, Indonesia, have yielded fossils of hominins[1] attributed to a population ancestral to Late Pleistocene *Homo floresiensis*[2]. Here we describe the context and age of the Mata Menge hominin specimens and associated archaeological findings. The fluvial sandstone layer from which the *in situ* fossils were excavated in 2014 was deposited in a small valley stream around 700

thousand years (kyr) ago, as indicated by $^{40}Ar/^{39}Ar$ and fission track dates on stratigraphically bracketing volcanic ash and pyroclastic density current deposits, in combination with coupled Uranium-series (U-series) and Electron Spin Resonance (ESR) dating of fossil teeth. Palaeoenvironmental data indicates a relatively hot and dry climate in the So'a Basin during the early Middle Pleistocene, while various lines of evidence suggest the hominins inhabited a savannah-like open grassland habitat with a strong wetland component. The hominin fossils occur alongside the remains of an insular fauna and a simple, 'Mode 1'-like stone technology that is markedly similar to that of *H. floresiensis*.

Mata Menge is located near the northwestern margin of the So'a Basin, a ~400 km^2 geological depression in the interior highlands of central Flores (Fig. 1). The basement substrate consists of the Ola Kile Formation (OKF), a >100 m-thick sequence of indurated volcaniclastic deposits dominated by andesitic breccia and locally alternating with lava flows, tuffaceous sandstones, and siltstones[3,4]. Zircon fission-track (ZFT) age determinations date the upper part of the OKF to 1.86 ± 0.12 million years ago (Ma) (ref. 4). The OKF is unconformably overlaid by the Ola Bula Formation (OBF) [3,4]. The latter is up to 120 m thick, and comprises an intra-basinal fossil- and stone artefact-bearing sequence deposited between 1.8 to 0.5 Ma. The ~5° southward dipping volcanic breccias of the OKF are associated with a former volcanic centre located on the northwestern edge of the basin. Inside the remnant of this 10 km diameter caldera structure, known as the Welas Caldera, are well-formed intra-caldera lake sediments punctuated by two intra-caldera basaltic cones that were the major sources of primary and secondary basaltic volcaniclastic deposits within the OBF.

Since the 1950s, palaeontological and archaeological research in the So'a Basin has focused on the OBF[5-14], which is composed largely of undistorted volcanic, fluvial, and lacustrine sediments[3,4]. The volcaniclastic aprons that entered the central depression from various directions, at times debouching into a lake, or series of small lakes, were incised by erosional gullies during periods of volcanic quiescence, but became sites of enhanced accretion following major volcanic influxes. Well-developed paleosols and pedogenically altered fine-grained fluviatile deposits intervening between variably textured pyroclastic (primary) and fluvio-volcaniclastic (secondary) deposits document intermittent periods of landscape stability that alternated with rapid depositional events triggered by major volcanic eruptions, generating airfall tephra, ignimbrites, and associated mass-flow deposits (see SI Table 1). A basin-wide, thinly-bedded lacustrine sequence, consisting of an alternation of thin-bedded micritic freshwater limestones, clays, and with numerous basaltic tephra inter-beds – the 'Gero Limestone Member' (GLM) – caps the basin infill and registers the formation of a basin-wide lake[3,4], which formerly extended into the Welas Caldera.

The total preserved thickness of the OBF at Mata Menge, up to the top of an adjacent hill northwest of the site, is 40 m (Fig. 1). The uppermost interval of the GLM, with a thickness of 9 m, outcrops at the summit of a hill 600 m west (Excavation #35, or E-35). The main fossil-bearing intervals at Mata Menge form part of a roughly NNW-SSE trending palaeovalley dominantly occupied by a sequence of cut-and-fill fluviatile and clay-rich mass-flow deposits. The hominin-bearing sedimentary layer lies at the head of a modern dry stream valley at the base of a hill (ht = 397m). A slot-trench excavated into the eastern side of this hill revealed an 18 m-thick sequence of planar bedded lacustrine clays and micritic limestones containing oogonia and diatoms, fluvial sandstone beds, massive tuffaceous clay-rich mass-flow (mudflow) deposits, fine-grained well-developed clay-textured paleosols, and numerous centimetre-thick basaltic tephra inter-beds, pertaining to the middle upper part of the OBF. At the base of this slot-trench, a thin (<30 cm-thick) fossil-bearing fluvial sandstone layer was exposed underlying a sequence of mudflow deposits (Layers Ia-f) up to 6.5 m thick. This fossiliferous sandstone, named Layer II, represents the deposit of a small stream channel that has an irregular lower bedding plane and was incised into a well-developed, consolidated paleosol with prominent root traces (Layer III).

We conducted a 50 m^2 excavation (E-32) into Layer II in 2013 (Fig. 1 and Extended Data Figs. 1-2). The sandstone layer yielded fossils of the dwarfed proboscidean *Stegodon florensis*[8], and numerous well-preserved dental and skeletal remains of giant rat (*Hooijeromys nusatenggara*)[15], as well as teeth of Komodo dragon (*Varanus komodoensis*) and crocodiles, and flaked stone artefacts (Fig. 2). In 2014, we exposed Layer II over a larger area by extending the initial trench (E-32A) to the south (E-32B/C) and west (E-32D/E). A separate excavation was also opened upstream of the palaeo-channel to the north (E-32F). These excavations recovered six hominin teeth and a hominin mandible fragment from Layer II (ref. 1). Another less diagnostic hominin fossil comprises a 60 mm^2 piece of a cranial vault. The hominin fossils occurred at the stratigraphic interface between Layer II and the overlying mudflow deposit, spread over a maximum linear distance of 15 m. The flow direction in the sinuous stream tributary in which Layer II was deposited was from NNW to SSE, based on the slight decrease in elevation of the top of this layer in the same direction (i.e., 20 cm over a horizontal distance of 17 m). The fine- to medium-grained fluvial sandstone has a maximum thickness of 30 cm, contains scattered pebbles, and occurs

13 m stratigraphically above the main (lower) fossil-bearing beds at Mata Menge, which have a combined thickness of up to two metres (Fig. 1).

The mudflow sequence (Layers Ia-f) sealing in Layer II can be clearly related to phreatomagmatic to magmatic eruptive activity occurring within the confines of the Welas Caldera (then occupied by a lake). The formation of these multiple mudflow events either relates to intermittent displacement of lake waters down adjacent tributaries during cone construction, or, alternatively, failure of a lake outlet barrier during and/or following intra-caldera eruptive activity. Four articulated thoracic vertebrae of *S. florensis* were recovered from Layer II (Fig. 2k) near a concentration of other vertebrae, ribs, and postcranial remains of a *Stegodon* carcass. These are the only articulated stegodont elements so far recovered at Mata Menge, indicating relatively limited post-mortem modification prior to burial by mudflows. We infer that the artefacts and faunal remains, including the hominin elements, were exposed to weathering on the ground surface, and could have been transported short distances by the small stream, before a series of mudflows originating from the intra-caldera lake system were channelized within adjacent stream tributaries, inundating these valleys with metre-thick muddy debris. It is conceivable that the presence of elements from multiple hominin individuals, including two juveniles, and several individual stegodonts, could be the result of a volcanic event. However, other explanations are also possible and more research into taphonomic factors is needed.

A total of four new radiometric determinations, with ages in sequential order and in accordance with the stratigraphic sequence, as well as previously published estimates, provide a robust chronological framework for the hominin fossils (Fig. 1; see also

Supplementary Information). Near the base of the OBF at Mata Menge, a widespread ignimbritic marker bed (the Wolo Sege Ignimbrite; T-WSI) with an $^{40}Ar/^{39}Ar$ age of 1.01 ± 0.02 Ma (ref. 13; and see Fig. 1) is recognised on the combined basis of its stratigraphic association, unique depositional architecture, and glass-shard major element chemistry (see Extended Data Fig. 3). In addition, the hominin find-locality in E-32 is situated 12.5 m stratigraphically above a ZFT date of 0.80 ± 0.07 Ma from Mata Menge[4]. To verify this prior estimate[4], we conducted Isothermal Plateau Fission-Track (ITPFT) dating of glass shards from an inter-regional tephra marker (T3) identified at several So'a Basin localities, including just above the T-WSI at Mata Menge (in E-34/34B), returning a weighted mean age of 0.90 ± 0.07 Ma (based on two independent age determinations) (see Extended Data Fig. 3). Moreover, $^{40}Ar/^{39}Ar$ single crystal dating of hornblende from the Pu Maso Ignimbrite (T-Pu) located just above T3 in E-34/34B yielded a weighted mean age of 0.81 ± 0.04 Ma, which is stratigraphically consistent with that of underlying T3 (Extended Data Fig. 4). These ages demonstrate that Layer II was deposited after ~0.80 Ma.

To further constrain the age of the hominin fossils, we carried out $^{40}Ar/^{39}Ar$ dating on one basaltic tephra and one rhyolitic tephra from the GLM above Layer II (E-12 and E-35). The GLM contains at least 85 crystal-rich tephra inter-beds of basaltic composition, collectively named the Piga Tephra (the lower 56 tephras are sequentially numbered PGT-1 to PGT-56). At Mata Menge, PGT-2 occurs 13.5 m above Layer II, and produced a $^{40}Ar/^{39}Ar$ weighted mean age of 0.65 ± 0.02 Ma from single crystal dating of hornblende (Extended Data Fig. 5). This is in accordance with the published ZFT age of a basaltic tephra inter-bed from the lower part of the GLM (0.65 ± 0.06 Ma)[4]. Finally, a biotite-bearing vitric-rich ash of distinctive rhyolitic composition (T6; see Extended Data Fig. 3) from the top of the GLM has an $^{40}Ar/^{39}Ar$ age of 0.51 ± 0.03 Ma, based on the weighted mean of single grain feldspar analyses. Thus, the hominin fossils constrained by the lowermost of these two radiometric dates within the GLM have an established minimum age of ~0.65 Ma.

In order to demonstrate that the hominin fossils and associated faunal assemblage do not reflect vertical displacement of chronologically more recent finds into older sediments, we conducted laser ablation U-series analysis of a hominin tooth root fragment from Layer II (specimen SOA-MM6), and combined U-series/ESR-dating of two *S. florensis* molars excavated *in situ* from the same sedimentary context (see Extended Data Fig. 7 and Supplementary Information). U-series dating of the hominin tooth root independently confirms this specimen was deposited at least 0.55 Ma, whereas combined U-series/ESR indicates minimum and maximum ages of around 0.36 Ma and 0.69 Ma, respectively, for the *Stegodon* molars. In sum, therefore, we have used multiple dating methods to establish a secure age of ~0.70 Ma for the Layer II hominin fossils.

Our systematic, high-volume excavations (~560 m^2) at Mata Menge between 2010–15 have yielded a wealth of fossil vertebrate remains (see Supplementary Information). To date, 75% of the >7000 vertebrate fossils recovered from E-32 have been analyzed, and include *S. florensis* (23.7% of the number of identified specimens, or NISP), *V. komodoensis* (0.6% of NISP), freshwater crocodiles (3.7% of NISP), frogs (0.3% of NISP), murine rodents (15.6 % of NISP), and birds (0.5% of NISP), the remainder comprising unidentifiable bone fragments. From the lower fossil-bearing interval (E-1 to 8 and E-11 to 31D) the remains of least 120 *S. florensis* individuals are represented by dental elements spanning all ontogenetic stages[16]. The age profile of the Mata Menge lower level death assemblage corresponds to that of a living population, suggesting a mass death event. The lack of age-selective mortality does not fit a pattern of hominin predation, such as in the *H. floresiensis* type-locality, Liang Bua[17]. In Layer II, remains of juvenile, sub-adult, intermediate-aged, and very old *Stegodon* individuals are also present, but the Minimum Number of Individuals is too low to allow for the construction of a reliable age profile.

We conducted carbon and oxygen isotope analysis of tooth enamel samples collected from several *S. florensis* and murine rodent individuals from the two fossil-bearing levels at Mata Menge (Extended Data Fig. 8). The results indicate a diet heavily dominated by C_4 grasses, suggesting both animals were grazers, and implying that open grasslands were the major vegetation type in the So'a Basin. The recovery of rare fossils of rails, swans, ducks, eagles, and eagle owls from the lower trenches (~0.80 to 0.88 Ma) further evidences the presence of a savannah-like biome with a strong wetland component, as well as scattered patches of forest[18]. Fossil pollen and phytoliths from both fossil levels, while poorly preserved, offer additional evidence that grasses dominated the Middle Pleistocene vegetation (SI Table 9). Abundant moulds and casts of two species of freshwater gastropods (Cerithoidea) were recovered from Layer II and the base of the overlying mudflow sequence, pointing to the existence of permanent freshwater bodies in the ancestral stream valley.

Our excavations uncovered 149 *in situ* stone artefacts in E-32, including 47 artefacts from Layer II, in direct association with the hominin remains (Fig 2; Extended Data Fig. 9). Some of the artefacts from E-32 are lightly to heavily abraded from lowenergy water transport[19], but 74.5% are in fresh, as-struck condition, suggesting minimal dislocation from nearby stone-flaking areas. Hominins gathered coarse- to fine-grained rounded volcanic cobbles from local fluvial gravels and struck them with hammerstones to create sharp-edged flakes and cores. Reduction was mostly bifacial, with blows struck to two faces of the stone from one platform edge (Fig 2a). Two cores were rotated and a second bifacial platform edge was established, resulting in multi-platform cores. Core platform surfaces or edge-angles were unprepared, and core reduction was not intensive. The edges of flakes struck from these cores were sometimes retouched for use, or possibly to produce additional flake tools. One heavily abraded core was scavenged and further flaked. Overall, the E-32 assemblage reflects a technologically straightforward core-and-flake approach to stoneworking[20]. The function of the implements is unknown; as yet, no butchery marks have been conclusively identified on the faunal remains at Mata Menge, and the tools may have been used for modifying other organic materials.

Notably, the tools and flaking technology in E-32 are nearly identical in size and nature, respectively, to the assemblage dating some 110 kyr earlier at Mata Menge[12,21-23], including 1186 analysed stone artefacts from E-23 and E-27 excavated between 2011–14 (Table S6). The E-32 assemblage is also technologically similar to the artefacts from Liang Bua, dating ~600 kyr later[12,24] and associated with *H. floresiensis*[25,26]. The long persistence of this technical approach to stone-flaking on Flores[12], together with the close anatomical similarities between the Mata Menge and Liang Bua hominins[1], suggests remarkable stability in the behaviour of the *H. floresiensis* lineage. In contrast, the only lithic assemblage thus far recovered *in situ* below the T-WSI, which has a minimum age of 1.01 ± 0.02 Ma and is therefore the earliest known stone technology from Flores[13], whilst also ‘Mode 1’ in character, features a typologically distinct element: large Acheulean pick-like implements[27] that in Lower Palaeolithic industries of Africa and western Eurasia are emblematic of cognitively advanced tool-making[20,28-29]. The reason for the absence of these more sophisticated components from the later technology of Flores remains unknown; however, possible explanations include: i) a reduction in the behavioural flexibility of *Homo erectus* due to island-dwarfing[1]; ii) by ~880 Ma the hominin population size had dropped below a minimum threshold required to maintain cultural complexity[30]; iii) the older, Acheulean-like artefacts were made by a separate hominin lineage.

References

1. van den Bergh, G. D. *et al*. *Homo floresiensis*-like hominin fossils from the Middle Pleistocene of Flores. *Nature* (submitted).

2. Brown, P. *et al*. A new small-bodied hominin from the Late Pleistocene of Flores, Indonesia. *Nature* **431**, 1055–1061 (2004).

3. Morwood, M. J. O’Sullivan, P. B., Aziz, F. & Raza, A. Fission-track ages of stone tools and fossils on the east Indonesian island of Flores. *Nature* **392**, 173–176 (1998).

4. O’Sullivan, P. B. *et al.* Archaeological implications of the geology and chronology of the Soa Basin, Flores, Indonesia. *Geology* **29**, 607–610 (2001).

5. Maringer, J. & Verhoeven, Th. Die Steinartefakte aus der *Stegodon*-Fossilschicht

von Mengeruda auf Flores, Indonesien. *Anthropos* **65**, 229–247 (1970).

6. Maringer, J. & Verhoeven, Th. Die Oberflächenfunde aus dem Fossilgebiet von Mengeruda und Olabula auf Flores, Indonesien. *Anthropos* **65**, 530–546 (1970).

7. Sondaar, P. Y. *et al.* Middle Pleistocene faunal turn-over and colonisation of Flores (Indonesia) by *Homo erectus*. *C.R. Acad. Sci.* **319**, 1255–1262 (1994).

8. Morwood, M. J. *et al.* Stone artefacts from the 1994 excavation at Mata Menge, West Central Flores, Indonesia. *Aust. Archaeol.* **44**, 26–34 (1997).

9. van den Bergh, G. D. *The Late Neogene Elephantoid-Bearing Faunas of Indonesia and their Palaeozoogeographic Implications. A Study of the Terrestrial Faunal Succession of Sulawesi, Flores and Java, including Evidence for Early Hominid Dispersal East of Wallace's Line* (Scripta Geologica 117, Nationaal Natuurhistorisch Museum, 1997).

10. van den Bergh, G. D. *et al*. Did *Homo erectus* reach the island of Flores? *Bull. Indo. Pac. Pre. Hi.* **14**, 27–36 (1996).

11. Morwood, M. J. *et al.* Archaeological and palaeontological research in central Flores, east Indonesia: results of fieldwork 1997-98. *Antiquity* **73**, 273–286 (1999).

12. Aziz, F. & Morwood, M. J., in *Pleistocene Geology, Palaeontology and Archaeology of the Soa Basin, Central Flores, Indonesia* (eds Aziz, F., Morwood, M.

J. & van den Bergh, G. D.) 1–18 (Spec. Publ. 36, Geological Survey Institute, 2009).

13. Brumm, A. *et al.* Early stone technology on Flores and its implications for *Homo floresiensis*. *Nature* **441**, 624–628 (2006).

14. Brumm, A. *et al.* Hominins on Flores, Indonesia, by one million years ago. *Nature* **464**, 748–753 (2010).

15. Musser, G. G. The giant rat of Flores and its relatives east of Borneo and Bali. *B. Am. Mus. Nat. Hist.* **169**, 67–176 (1981).

16. van den Bergh, G. D. *et al.* Taphonomy of *Stegodon florensis* remains from the early Middle Pleistocene archaeological site Mata Menge, Flores, Indonesia. Abstract book of the VIth International Conference on Mammoths and their relatives. *S.A.S.G., Special Volume* **102**, 207–208 (2014).

17. van den Bergh, G. D. *et al.* The Liang Bua faunal remains: a 95 k.y.r. sequence from Flores, East Indonesia. *J. Hum. Evol.* **57**, 527–537 (2009).

18. Meijer, H. J. M. *et al*. Avian remains from the Early/Middle Pleistocene of the So'a Basin, central Flores, Indonesia, and their palaeoenvironmental significance. *Palaeogeogr. Palaeocl.* **440**, 161–171 (2015).

19. Shea, J. J. Artifact abrasion, fluvial processes, and ''living floors'' from the Early Paleolithic site of 'Ubeidiya (Jordan Valley, Israel). *Geoarchaeology* **14**, 191–207

(1999).

20. Moore, M. W. The design space of stone flaking: implications for cognitive evolution. *World Archaeol*. **43**, 702–715 (2011).

21. Brumm, A. *et al.* Stone technology at the Middle Pleistocene site of Mata Menge, Flores, Indonesia. *J. Arch. Sci.* **37**, 451–473 (2010).

22. Moore, M. W. & Brumm, A. Stone artifacts and hominins in island Southeast Asia: new insights from Flores, eastern Indonesia*. J. Hum. Evol.* **52**, 85–102 (2007).

23. Moore, M. W. & Brumm, A. in *Interdisciplinary Approaches to the Oldowan* (eds Hovers, E. & Braun, D. R.) 61–69 (Springer, 2009).

24. Moore, M.W. *et al.* 2009. Continuities in stone flaking technology at Liang Bua, Flores, Indonesia. *J. Hum. Evol.* **57**, 503–526 (2009).

25. Morwood, M. J. *et al.* Archaeology and age of a new hominin from Flores in eastern Indonesia. *Nature* **431**, 1087–1091 (2004).

26. Sutikna, T. *et al.* Revised stratigraphy and chronology for *Homo floresiensis* at Liang Bua, eastern Indonesia. *Nature* (under review).

27. Brumm, A. & Moore, M. W. Biface distributions and the Movius Line: a Southeast Asian perspective. *Aust. Archaeol.* **74**, 32–46 (2012).

28. Beyene, Y. *et al.* The characteristics and chronology of the earliest Acheulean at Konso, Ethiopia. *Proc. Natl Acad. Sci. USA* **110**, 1584–1591 (2013).

29. Wynn, T. Archaeology and cognitive evolution. *Behav. Brain Sci.* **25**, 389–402 (2002).

30. Powell, A. *et al.* Late Pleistocene demography and the appearance of modern human behavior. *Science* **324**, 1298–1301 (2009).

Supplementary Information is available in the online version of the paper.

Acknowledgments

The So’a Basin project was funded by an Australian Research Council (ARC) *Discovery* grant (DP1093342) awarded to M.J.M. and A.B., and directed by M.J.M. (2010-2013) and G.v.d.B. (2013-2015), while the Geological Survey Institute (GSI) of Bandung, Indonesia, provided financial and technical support. G.v.d.B.’s research was also supported by ARC Future Fellowship FT100100384. Quadlab is funded by a grant to M.S. from the Villum Foundation. M.D. received funding from a Marie Curie International Outgoing Fellowship of the EU’s Seventh Framework Programme (FP7/2007-2013), awarded under REA Grant Agreement No. PIOF-GA-2013-626474. For permission to undertake this research, we thank the Indonesian State Ministry of Research and Technology (RISTEK), the former Heads of the Geological Agency (R. Sukyiar and Surono), the successive directors of the GSI (S.

Permanandewi, Y. Kusumahbrata [formerly] and A. Pribadi) and Bandung's Geology Museum (S. Baskoro and O. Abdurahman). Local research permissions were issued by the provincial government of East Nusatenggara at Kupang, and the Ngada and Nage Keo administrations. We also thank the Ngada Tourism and Culture and Education Departments for their ongoing support. In addition, we acknowledge support and advice provided by I. Setiadi, D. Pribadi and Suyono (GSI), the National Centre for Archaeology (ARKENAS) in Jakarta, and J.T. Solo of the provincial Culture and Tourism office in Kupang. Scientific and technical personnel involved in the fieldwork included: T. Suryana, S. Sonjaya, H. Oktariana, I. Sutisna, A. Rahman, S. Bronto, E. Sukandar, A. Gunawan, Widji, A.S. Hascaryo, Jatmiko, S. Wasisto, R.A. Due, S. Hayes, Y. Perston, B. Pillans, K. Grant, M. Marsh, D. McGahan, A.M. Saiful, Basran, M. Tocheri, A. R. Chivas and S. Flude. Sidarto (GSI) provided DEM data used in Fig. 1b. Geodetic surveys and measurements were conducted by E.E. Laksmana, A. Rahmadi and Y. Sofyan. J. Noblett constructed the Mata Menge 3D model, based on drone aerial photographs taken by K. Riza, T.P. Ertanto, and M. Faizal. The research team was supported by ~100 excavators and support personnel from the Ngada and Nage Keo districts. R.G. and M.D. thank L. Kinsley, RSES, The Australian National University, for his assistance with the mass spectrometric measurements.

Author contributions

A.B., G.D.v.d.B., I.K. and M.J.M. directed the Mata Menge excavations. M.S., B.A. and R.S. collected tephra samples and M.S. undertook ^{40}Ar/^{39}Ar dating.

G.D.v.d.B. described the site stratigraphy, with R.S., D.Y. and B.V.A.. J.A.W.

conducted ITPFT-dating of T3 with B.V.A. and comparative trace element analyses of interregional markers (with N.J.P. & B.V.A.). E.S., F.A. and T.S. oversaw key aspects of the field project. M.W.M. analysed the stone assemblage, and G.D.v.d.B., H.I., I.S., M.R.P. U.P.W. and H.J.M.M. analysed the fauna. M.P. conducted isotopic analyses, R.G. and M.D. undertook U/Th and ESR analyses of faunal remains, and S.v.d.K. carried out the palynological analysis. A.B. and G.D.v.d.B. prepared the manuscript, with contributions from other authors.

Figure legends (main text)

Figure 1: Context and chronology of the hominin fossils at Mata Menge. **a**-**b**, location of Flores and the So'a Basin; **c**, Digital Elevation Map of the So'a Basin, showing the location of Mata Menge and other sites mentioned in the text. A single outlet of the main river system (the Ae Sissa) drains the basin via a steep-walled valley towards the northeast; **d**, stratigraphy and chronology of the main fossil-bearing intervals and intervening Ola Bula Formation (OBF) deposits at Mata Menge. Several basin-wide key marker tephra beds that are exposed in the hill flank on the northern side of Mata Menge (trench E-34/34B) are eroded in the central part of the stream valley, where they are replaced by a 4-5 m thick sequence of tuffaceous mudflows with intervening fluvial lenses forming the lower fossil-bearing paleovalley-fill sequence; **e**-**f**, context of the hominin fossils; **f** is a 3D image of Mata Menge and surrounds, with excavated trenches outlined in red and labelled, and **e** is a 3D representation of the stratigraphy exposed by trench E-32A-E, with coloured ovals denoting the positions of *in situ* hominin fossils (SOA-MM1, 2 and 4-6) excavated from the fluvial sandstone unit, Layer II. Trenches E-1 to E-8 were excavated

between 2004-06, at the section originally excavated by Th. Verhoeven in the 1950s[5,6]. The remaining trenches were excavated between 2010 to 2015. Tephra codes in **d** are as follows (top to bottom): T6 (upper inter-regional tephra); PGT-2 (Piga Tephra 2); T-UMM (Upper Mata Menge Tephra); T-LMM (Lower Mata Menge Tephra); T-Pu (Pu Maso Tephra); T3 (lower inter-regional tephra); T-T (Turakeo Tephra); T-WSI (Wolo Sege Ignimbrite); T-W (Wolowawu Tephra). The original published ^{40}Ar/^{39}Ar age for T-WSI is 1.02 ± 0.02 Ma (ref. 13); however, when recalculated to the recently determined value for the age standard ACS-2 used in this study (1.185 Ma; see SI ref. 25), T-WSI becomes 1.01 ± 0.02 Ma.

Figure 2: Stone artefacts and fossils from Mata Menge. All specimens are from the hominin fossil find-locality (Layer II fluviatile sandstone, Trench E-32). **a**, bifacial core (chlorite); **b-c**, chert flakes; **d**, chalcedony flake; **e**, rhyolite flake; **f**, right maxilla fragment (M1-M3), *Hooijeromys nusatenggara*; **g**, left mandible fragment (m1-m3, i) *H. nusatenggara*; **h**, right maxilla fragment, *Varanus komodoensis*; **i**, crocodile tooth; **j**, right coracoid of a duck (cf. *Tadorna*); **k**, *Stegodon florensis* thoracic vertebrae in articulation (still partially embedded in sandstone matrix). Scale bar lengths: **a-i** = 10 mm; **j** = 100 mm.

Figure legends (extended data)

Extended Data Figure 1. Hominin fossil find-locality at Mata Menge. a, View of Excavation 32 (trench E-32) in 2014, taken towards the north-north-west. The dip slope visible in the background is the eastern flank of the Welas Caldera, which was the source for many of the volcanic products deposited in the So'a Basin; **b**, E-32A-E viewed towards the southwest, in October 2015; **c**, E-32D to E-32E viewed towards the southwest. The irregular erosional upper surface of the reddish brown paleosol (Layer III) formed the hardened bedding of a small stream. The sandy fossil-bearing Layer II infills depressions formed on this bedding surface. A sequence of mudflows (Layer I/a-f) rapidly covered the entire river bedding and its exposed banks; **d**, Mold of a freshwater gastropod (Cerithoidea) from a sandy lens in Layer II; **e**, Detail of the locally developed, gradual boundary between sandy Layers II and muddy Layer I. Note the abundance of muddy rip clasts around the transition. At other places, the boundary is sharp; **f**, West baulk of E-32C. Large *Stegodon florensis* bones occur at the boundary between Layers II and I.

Extended Data Figure 2: Plan and baulk profiles of Excavation 32A-F showing distribution of finds. The horizontal plan (lower left corner) shows the horizontal coordinates of individual fossil finds (green crosses) and stone artefacts (blue diamonds). The original position of hominin fossils is indicated with red stars. In the trench baulk profiles (top and right) only the projected positions of fossil finds occurring within one meter of the baulks are plotted. All hominin fossils were recovered from the top of sandy Layer II. The basal part of the mudflow unit (Layers Ia-e) also contains fossils, stone artefacts, gastropods, and pebbles. The thick brown dotted line indicates the western margin of the ancient streambed.

Extended Data Figure 3: ITPFT dating and glass chemistry analysis. a-c, Selected major element compositions (weight percent FeO vs. K_2O and CaO and SiO_2 vs. K_2O) of glass shards from key rhyolitic pyroclastic density current (PDC) and airfall deposits at Mata Menge; **d-h,** Weight percent FeO versus CaO composition of glass shards from key rhyolitic pyroclastic density current (PDC) and airfall deposits at Mata Menge (in stratigraphic sequence – youngest to oldest) compared with correlatives from adjacent So'a Basin sites. While the major element glass compositions of T-WSI, T-T and T-Pu are all geochemically indistinguishable (i.e., they are most likely from the same eruptive source) the major element data for each of the tephra consistently occupies different overlapping fields. Moreover, while subtle geochemical differences exist between T-WSI, T-T and T-Pu, these tephra can also be readily distinguished in the field by a combination of stratigraphic position and association, as well as by morphological expression; **i-j**, Selected trace element compositions Sr versus Th and Zr, and (**k-m**) Y versus Nb, Ce and Th of glass shards from T3 correlatives at Mata Menge, Lowo Mali and Kopowatu as well as T6 (uppermost inter-regional marker) from Mata Menge. All trace element concentrations are in ppm unless otherwise stated. This data is plotted against equivalent elemental mean and standard deviation (represented as ± 1σ error bars) reference data from potential distal tephra correlatives (i.e. Youngest Toba Tuff [YTT], Middle Toba Tuff [MTT], Oldest Toba Tuff [OTT] and Unit E from ODP-758) acquired on the same instrument using the same standards and under the same analytical conditions[31,32]. Trace element data indicates that the upper (T6) and lower (T3) inter-regional marker beds occurring at Mata Menge cannot be geochemically related to any known Toba-sourced tephra. On this basis, the eruptive sources of T6 and T3 currently remain unknown. However, this absence of eruptive source certainly does not diminish their importance within the overall So'a Basin stratigraphy.

Extended Data Figure 4: ^{40}Ar/^{39}Ar dating results. **a**, Age probability plot for single crystal laser fusion data for hornblende from the Pu Maso ignimbrite (sample FLO-15-15; SI Table 5); the vertical scale is a relative probability measure of a given age occurring in the sample[33]. We applied an outlier-rejection scheme to the main population to discard ages with normalized median absolute deviations of >1.5 (ref. 34) and these are shown as open circles. %40Ar* refers to the proportion of radiogenic 40Ar released for individual analyses. The weighted mean age of the filtered hornblende data for the Pu Maso ignimbrite is 0.81 ± 0.04 Ma (1□□□mswd = 0.59, prob = 0.93; n = 23/29). An inverse isochron plot (**b**) for these 23 analyses gives a statistically overlapping age of 0.78 ± 0.07 Ma (1σ; mswd = 0.6, prob. = 0.92). The ^{40}Ar/^{36}Ar intercept of 303 ± 10 is statistically indistinguishable from the atmospheric ratio of 298.6 ± 0.3 (ref. 35), thus supporting the more precise weighted mean age result.

Extended Data Figure 5: ^{40}Ar/^{39}Ar dating results. **a**, Age probability plot for single crystal laser fusion data for hornblende from the PGT-2 tephra (sample T XII 252-261; SI Table 5). ^{40}Ar* ranges from < 10% to nearly 60%. The weighted mean age of the filtered hornblende data for the PGT-2 tephra is 0.65 ± 0.02 Ma (1σ; mswd = 0.78, prob = 0.71; n = 17/24). An inverse isochron plot (**b**) gives a statistically overlapping, but less precise age of 0.61 ± 0.04 Ma (1σ; mswd = 1, prob. = 0.19).

Extended Data Figure 6: ^{40}Ar/^{39}Ar dating results. **a**, Age probability plot for single crystal laser fusion data for anorthoclase from the T6 upper inter-regional rhyolitic tephra (sample FLO15-09/2; SI Table 5). ^{40}Ar* ranges from 20% to nearly 100%. The weighted mean age of the filtered feldspar data for the T6 tephra is 0.51 ± 0.03 Ma (1σ; mswd = 0.20, prob = 0.94; n = 5/8). An inverse isochron plot (**b**) gives a statistically overlapping, but less precise age of 0.45 ± 0.04 Ma (1σ; mswd = 0.8, prob. = 0.54).

Extended Data Figure 7: U-series and ESR samples and dating results. a, Hominin tooth root samples (#3543A and #3543B) from Layer II, Mata Menge; **b**, **d**, U-series laser tracks for *Stegodon* molar samples from Layer II; **e**, **f**, Dose response curves obtained for the two powder enamel samples from #3541 and #3544, respectively. Fitting was carried out with a SSE function through the pooled mean ESR intensities derived from each repeated measurement. Given the magnitude of the D_E values, the correct D_E value was obtained for $5>D_{max}/D_E>10$ (ref. 36).

Extended Data Figure 8. Carbon and oxygen isotope analysis of dental enamel. a, $\delta^{13}C$ and $\delta^{18}O$ values of *Stegodon florensis* and murine rodent tooth enamel. All but one of the $\delta^{13}C$ ratios corresponds with a C_4 diet, indicating that both *Stegodon* and murine rodents were predominantly grazers in both fossil-bearing horizons. The positive shift observed in $\delta^{18}O$ of the younger *Stegodon* samples (from the hominin-bearing Layer II) is more difficult to interpret with the limited data available, but could mean a distinct source of drinking water (run-off versus lacustrine) and/or warmer conditions; **b**, Benferroni corrected p values for a pairwise Mann-Whitney statistical analysis to test for similarity of $\delta^{13}C$ between subsamples; **c**, Benferroni corrected p values for a pairwise Mann-Whitney statistical analysis to test for similarity of $\delta^{18}O$ between subsamples; p values showing significant differences in median values are in bold.

Extended Data Figure 9: Analytical data for the Mata Menge stone technology. **a**, Artefact counts and provenance, Trench E-32 (artefact definitions after ref. 37); **b**, raw materials used to manufacture the stone tool assemblage, Trench E-32; **c**, Platform types on flakes and modified flakes, E-32. Cortical: the blow was struck onto the cortical surface of a cobble. Single-facet: the blow was struck on a scar produced by previous reduction. Dihedral: the blow was struck on the ridge between two scars produced by previous reduction. Multifacet: the blow was struck on the surface of multiple small scars produced by previous reduction. Edge: the blow was struck on the edge of the core and a platform surface is not retained on the flake; **d**, Cortex coverage on the dorsal surface of complete unmodified flakes, E-32. Percent cortex coverage refers to the proportion of the dorsal surface covered in cortex; **e**, Artefact counts, Trenches E-32 and E-23/27 (artefact definitions after ref. 37); **f**, Sizes of artefacts and attributes, E-32 and E-23/27; **g**, Raw materials used to manufacture the stone tool assemblage, E-32 and E-23/27; **h**, Scatterplot of complete flake sizes, E-32 (total sample size [N] = 68 complete flakes) and E-23/27 (N=443). With regards to raw materials, coarse- and medium-grained materials include andesite, basalt, rhyolite, and tuff. Fine-grained materials include silicified tuff, chalcedony, and opal.

31. Pearce, N. J. G. *et al.* A compilation of new and published major and trace element data for NIST SRM 610 and NIST SRM 612 glass reference materials. *Geost. Newslet.* **21**, 115-144 (1997).

32. Pearce, N. J. G. *et al.* Trace-element analysis by LA- ICP-MS: the quest for comprehensive chemical characterisation of single sub-10um volcanic glass shards. *Quat. Int.* **246**, 57 - 81 (2011).

33. Deino, A. & Potts, R. Age-probability spectra for examination of single-crystal ^{40}Ar/^{39}Ar dating results: Examples from Olorgesailie, southern Kenya Rift. *Quat. Int.* **13–14**, 47–53 (1992).

34. Powell, R., Hergt, J. & Woodhead, J. Improving isochron calculations with robust statistics and the bootstrap. *Chem. Geol.* **185**, 191–204 (2002).

35. Lee, J.-Y. *et al.* A redetermination of the isotopic abundances of atmospheric Ar. *Geochim. Cosmochim. Acta* **70**, 4507–4512 (2006).

36. Duval, M. & Grün, R. Are published ESR dose assessments on fossil tooth enamel reliable? *Quat. Geochron.* **31**, 19–27 (2016).

37. Moore, M.W. *et al.* 2009. Continuities in stone flaking technology at Liang Bua, Flores, Indonesia. *J. Hum. Evol.* **57**, 503–526 (2009).

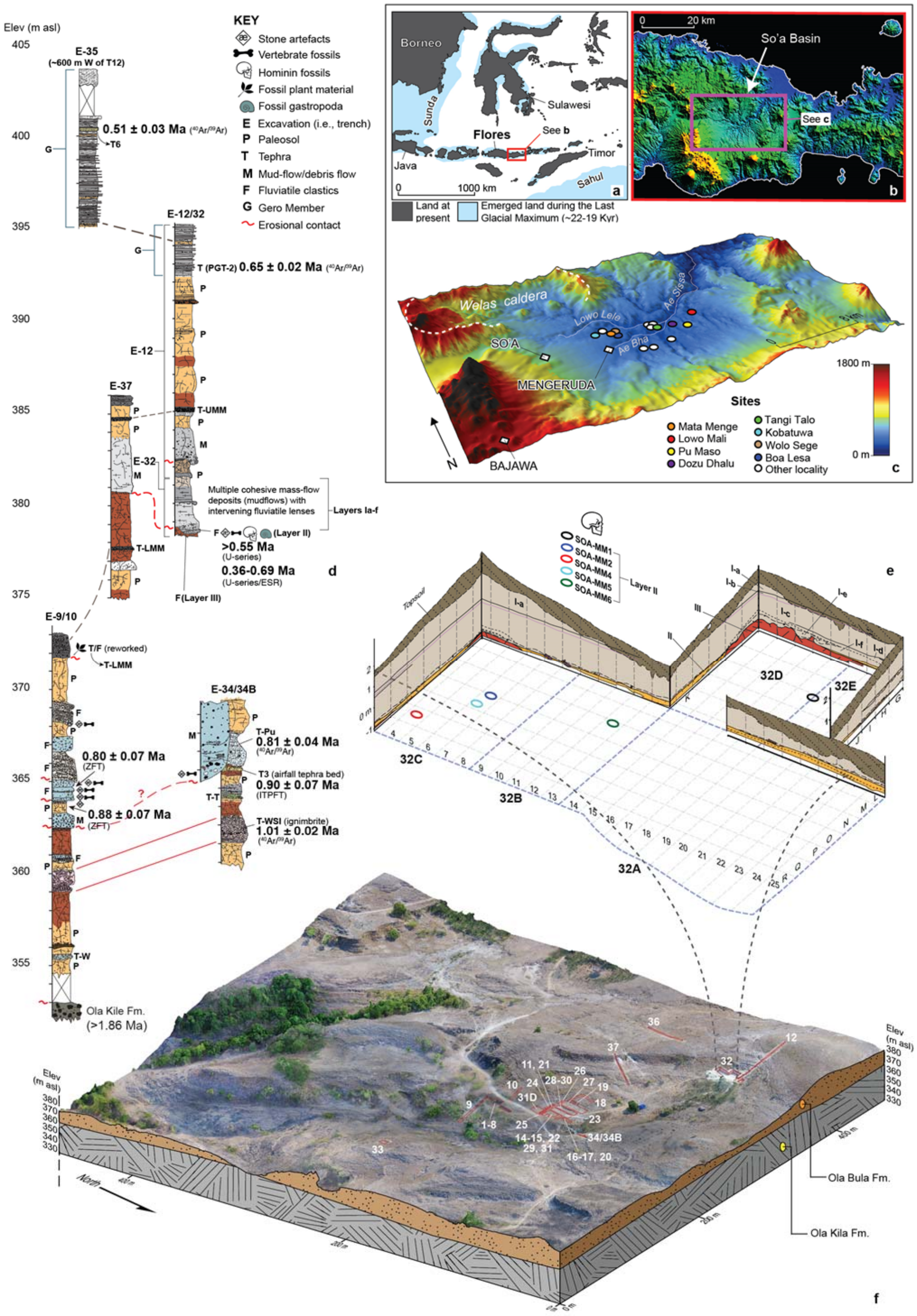

Figure 1: Context and chronology of the hominin fossils at Mata Menge. **a-b**, location of Flores and the So'a Basin; **c**, Digital Elevation Map of the So'a Basin, showing the location of Mata Menge and other sites mentioned in the text. A single outlet of the main river system (the Ae Sissa) drains the basin via a steep-walled

valley towards the northeast; **d**, stratigraphy and chronology of the main fossil-bearing intervals and intervening Ola Bula Formation (OBF) deposits at Mata Menge. Several basin-wide key marker tephra beds that are exposed in the hill flank on the northern side of Mata Menge (trench E-34/34B) are eroded in the central part of the stream valley, where they are replaced by a 4-5 m thick sequence of tuffaceous mudflows with intervening fluvial lenses forming the lower fossil-bearing paleovalley-fill sequence; **e**-**f**, context of the hominin fossils; **f** is a 3D image of Mata Menge and surrounds, with excavated trenches outlined in red and labelled, and **e** is a 3D representation of the stratigraphy exposed by trench E-32A-E, with coloured ovals denoting the positions of *in situ* hominin fossils (SOA-MM1, 2 and 4-6) excavated from the fluvial sandstone unit, Layer II. Trenches E-1 to E-8 were excavated between 2004-06, at the section originally excavated by Th. Verhoeven in the 1950s[5,6]. The remaining trenches were excavated between 2010 to 2015. Tephra codes in **d** are as follows (top to bottom): T6 (upper inter-regional tephra); PGT-2 (Piga Tephra 2); T-UMM (Upper Mata Menge Tephra); T-LMM (Lower Mata Menge Tephra); T-Pu (Pu Maso Tephra); T3 (lower inter-regional tephra); T-T (Turakeo Tephra); T-WSI (Wolo Sege Ignimbrite); T-W (Wolowawu Tephra). The original published $^{40}Ar/^{39}Ar$ age for T-WSI is 1.02 ± 0.02 Ma (ref. 13); however, when recalculated to the recently determined value for the age standard ACS-2 used in this study (1.185 Ma; see SI ref. 25), T-WSI becomes 1.01 ± 0.02 Ma.

Figure 2: Stone artefacts and fossils from Mata Menge. All specimens are from the hominin fossil find-locality (Layer II fluviatile sandstone, Trench E-32). **a**, bifacial core (chlorite); **b-c**, chert flakes; **d**, chalcedony flake; **e**, rhyolite flake; **f**, right maxilla fragment (M1-M3), *Hooijeromys nusatenggara*; **g**, left mandible fragment (m1-m3, i) *H. nusatenggara*; **h**, right maxilla fragment, *Varanus komodoensis*; **i**, crocodile tooth; **j**, right coracoid of a duck (cf. *Tadorna*); **k**, *Stegodon florensis* thoracic vertebrae in articulation (still partially embedded in sandstone matrix). Scale bar lengths: **a-i** = 10 mm; **j** = 100 mm.

Extended Data Figure 1. Hominin fossil find-locality at Mata Menge. a, View of Excavation 32 (trench E-32) in 2014, taken towards the north-north-west. The dip slope visible in the background is the eastern flank of the Welas Caldera, which was the source for many of the volcanic products deposited in the So’a Basin; **b**, E-32A-E viewed towards the southwest, in October 2015; **c**, E-32D to E-32E viewed towards the southwest. The irregular erosional upper surface of the reddish brown paleosol (Layer III) formed the hardened bedding of a small stream. The sandy fossil-bearing Layer II infills depressions formed on this bedding surface. A sequence of mudflows (Layer I/a-f) rapidly covered the entire river bedding and its exposed banks; **d**, Mold of a freshwater gastropod (Cerithoidea) from a sandy lens in Layer II; **e**, Detail of the locally developed, gradual boundary between sandy Layers II and muddy Layer I. Note the abundance of muddy rip clasts around the transition. At other places, the boundary is sharp; **f**, West baulk of E-32C. Large *Stegodon florensis* bones occur at the boundary between Layers II and I.

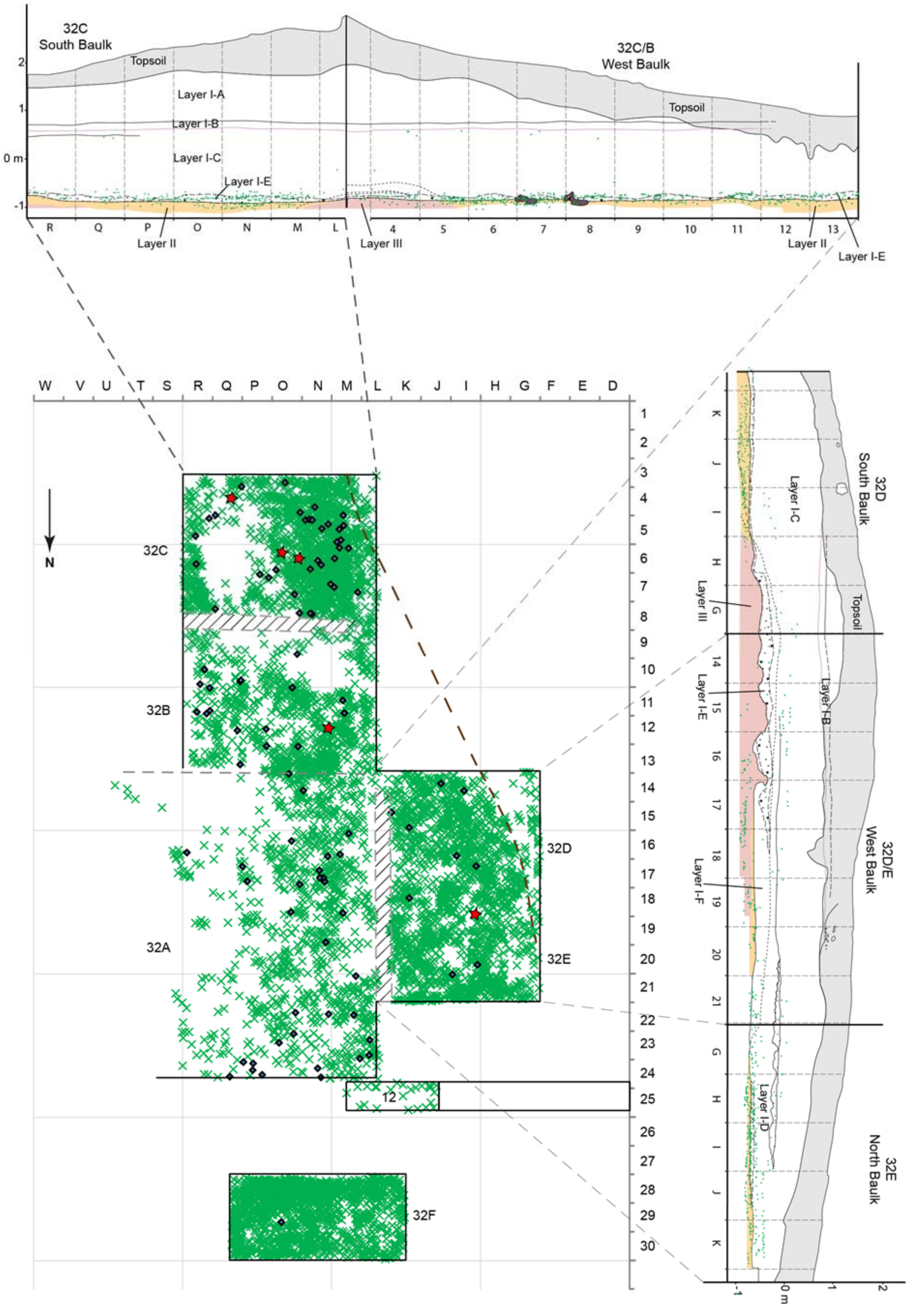

Extended Data Figure 2: Plan and baulk profiles of Excavation 32A-F showing distribution of finds. The horizontal plan (lower left corner) shows the horizontal coordinates of individual fossil finds (green crosses) and stone artefacts (blue diamonds). The original position of hominin fossils is indicated with red stars. In the trench baulk profiles (top and right) only the projected positions of fossil finds occurring within one meter of the baulks are plotted. All hominin fossils were recovered from the top of sandy Layer II. The basal part of the mudflow unit (Layers Ia-e) also contains fossils, stone artefacts, gastropods, and pebbles. The thick brown dotted line indicates the western margin of the ancient streambed.

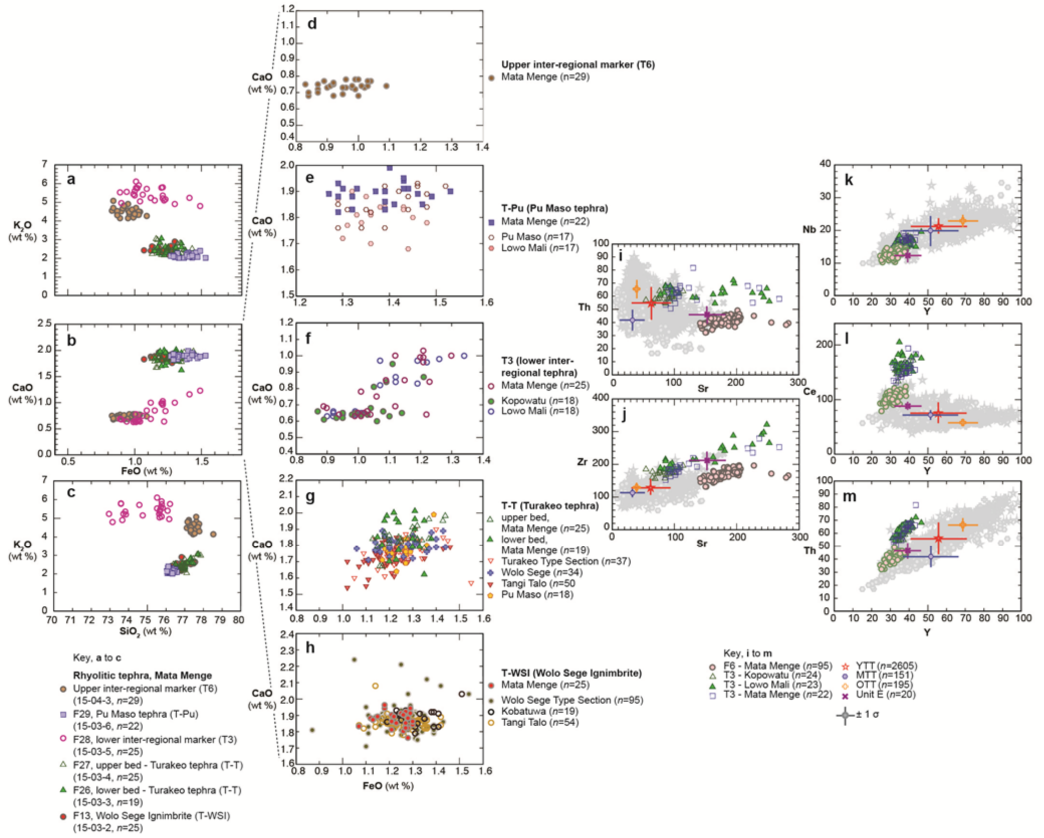

Extended Data Figure 3: ITPFT dating and glass chemistry analysis. a-c, Selected major element compositions (weight percent FeO vs. K_2O and CaO and SiO_2 vs. K_2O) of glass shards from key rhyolitic pyroclastic density current (PDC) and airfall deposits at Mata Menge; **d-h,** Weight percent FeO versus CaO composition of glass shards from key rhyolitic pyroclastic density current (PDC) and airfall deposits at Mata Menge (in stratigraphic sequence – youngest to oldest) compared with correlatives from adjacent So’a Basin sites. While the major element glass compositions of T-WSI, T-T and T-Pu are all geochemically indistinguishable (i.e., they are most likely from the same eruptive source) the major element data for each of the tephra consistently occupies different overlapping fields. Moreover, while subtle geochemical differences exist between T-WSI, T-T and T-Pu, these tephra can also be readily distinguished in the field by a combination of stratigraphic position and association, as well as by morphological expression; **i-j**, Selected trace element compositions Sr versus Th and Zr, and (**k-m**) Y versus Nb, Ce and Th of glass shards from T3 correlatives at Mata Menge, Lowo Mali and Kopowatu as well as T6 (uppermost inter-regional marker) from Mata Menge. All trace element concentrations are in ppm unless otherwise stated. This data is plotted against equivalent elemental mean and standard deviation (represented as ± 1σ error bars) reference data from potential distal tephra correlatives (i.e. Youngest Toba Tuff [YTT], Middle Toba Tuff [MTT], Oldest Toba Tuff [OTT] and Unit E from ODP-758) acquired on the same instrument using the same standards and under the same analytical conditions[31,32]. Trace element data indicates that the upper (T6) and lower (T3) inter-regional marker beds occurring at Mata Menge cannot be geochemically related to any known Toba-sourced tephra. On this basis, the eruptive sources of T6 and T3 currently remain unknown. However, this absence of eruptive source certainly does not diminish their importance within the overall So’a Basin stratigraphy.

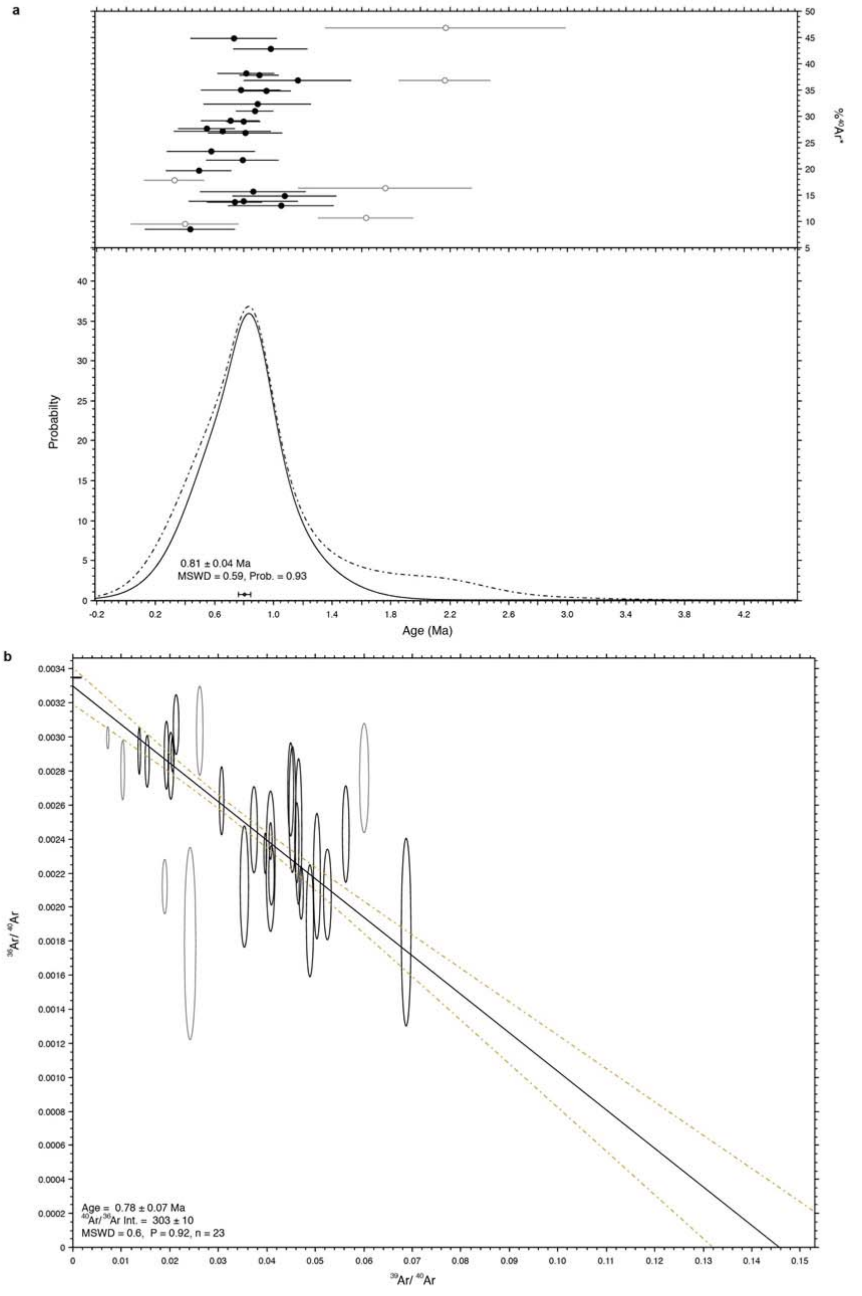

Extended Data Figure 4: ^{40}Ar/^{39}Ar dating results. **a**, Age probability plot for single crystal laser fusion data for hornblende from the Pu Maso ignimbrite (sample FLO-15-15; SI Table 5); the vertical scale is a relative probability measure of a given age occurring in the sample[33]. We applied an outlier-rejection scheme to the main population to discard ages with normalized median absolute deviations of >1.5 (ref. 34) and these are shown as open circles. %40Ar* refers to the proportion of radiogenic 40Ar released for individual analyses. The weighted mean age of the filtered hornblende data for the Pu Maso ignimbrite is 0.81 ± 0.04 Ma (1□□□mswd = 0.59, prob = 0.93; n = 23/29). An inverse isochron plot (**b**) for these 23 analyses gives a statistically overlapping age of 0.78 ± 0.07 Ma (1σ; mswd = 0.6, prob. = 0.92). The ^{40}Ar/^{36}Ar intercept of 303 ± 10 is statistically indistinguishable from the atmospheric ratio of 298.6 ± 0.3 (ref. 35), thus supporting the more precise weighted mean age result.

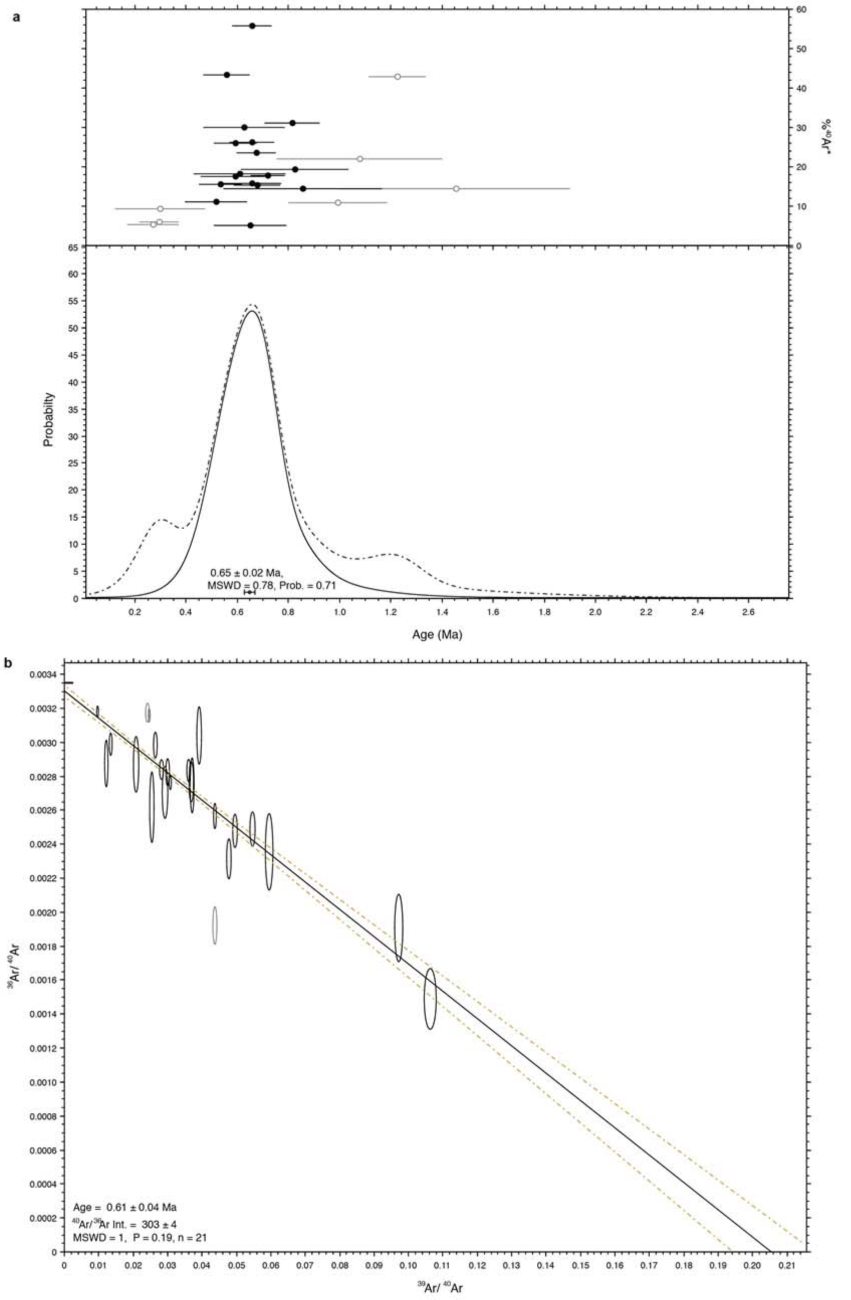

Extended Data Figure 5: ^{40}Ar/^{39}Ar dating results. **a**, Age probability plot for single crystal laser fusion data for hornblende from the PGT-2 tephra (sample T XII 252-

261; SI Table 5). ^{40}Ar* ranges from < 10% to nearly 60%. The weighted mean age of the filtered hornblende data for the PGT-2 tephra is 0.65 ± 0.02 Ma (1σ; mswd = 0.78, prob = 0.71; n = 17/24). An inverse isochron plot (**b**) gives a statistically overlapping, but less precise age of 0.61 ± 0.04 Ma (1σ; mswd = 1, prob. = 0.19).

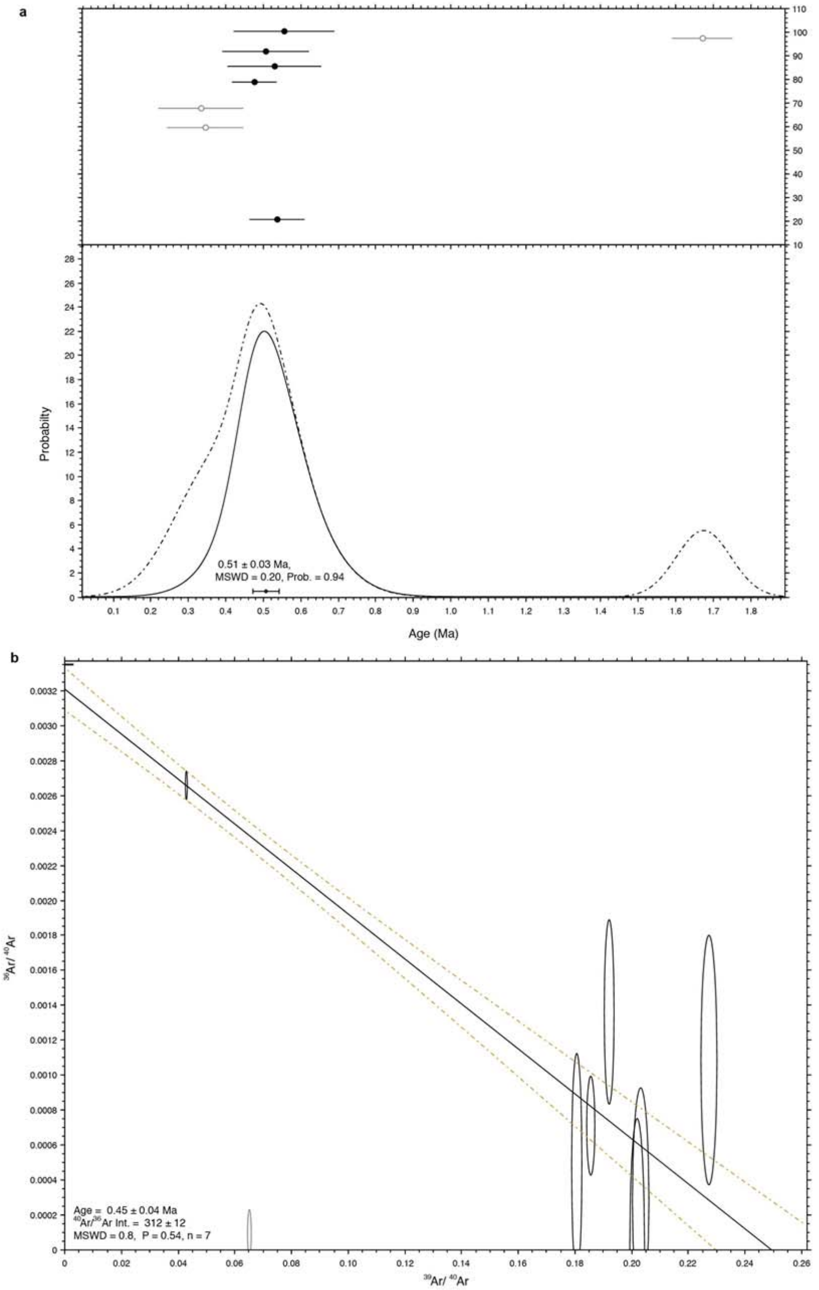

Extended Data Figure 6: ^{40}Ar/^{39}Ar dating results. **a**, Age probability plot for single crystal laser fusion data for anorthoclase from the T6 upper inter-regional rhyolitic tephra (sample FLO15-09/2; SI Table 5). ^{40}Ar* ranges from 20% to nearly 100%. The weighted mean age of the filtered feldspar data for the T6 tephra is 0.51 ± 0.03 Ma (1σ; mswd = 0.20, prob = 0.94; n = 5/8). An inverse isochron plot (**b**) gives a statistically overlapping, but less precise age of 0.45 ± 0.04 Ma (1σ; mswd = 0.8, prob. = 0.54).

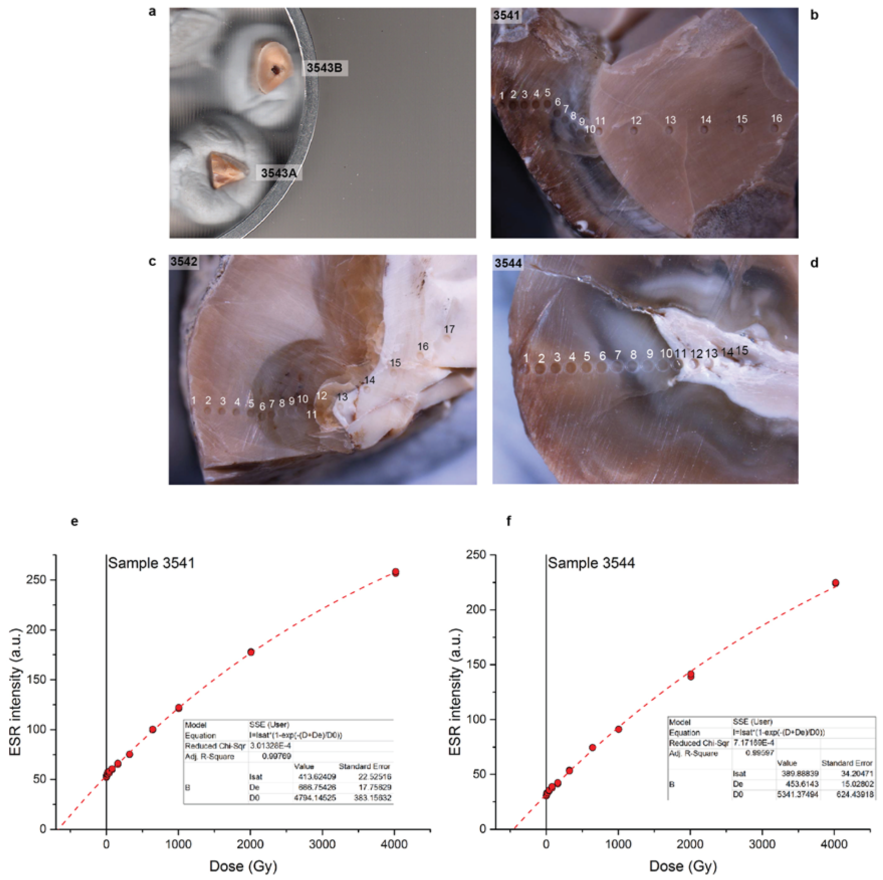

Model	SSE (User)		
Equation	I=Isat*(1-exp(-(D+De)/D0))		
Reduced Chi-Sqr	3.01328E-4		
Adj. R-Square	0.99769		
		Value	Standard Error
B	Isat	413.62409	22.52516
	De	686.75426	17.75829
	D0	4794.14525	383.15832

Model	SSE (User)		
Equation	I=Isat*(1-exp(-(D+De)/D0))		
Reduced Chi-Sqr	7.17160E-4		
Adj. R-Square	0.99597		
		Value	Standard Error
B	Isat	389.88839	34.20471
	De	453.6143	15.02802
	D0	5341.37494	624.43918

Extended Data Figure 7: U-series and ESR samples and dating results. a, Hominin tooth root samples (#3543A and #3543B) from Layer II, Mata Menge; **b**, **d**, U-series laser tracks for *Stegodon* molar samples from Layer II; **e**, **f**, Dose response curves obtained for the two powder enamel samples from #3541 and #3544, respectively. Fitting was carried out with a SSE function through the pooled mean ESR intensities derived from each repeated measurement. Given the magnitude of the D_E values, the correct D_E value was obtained for $5>D_{max}/D_E>10$ (ref. 36).

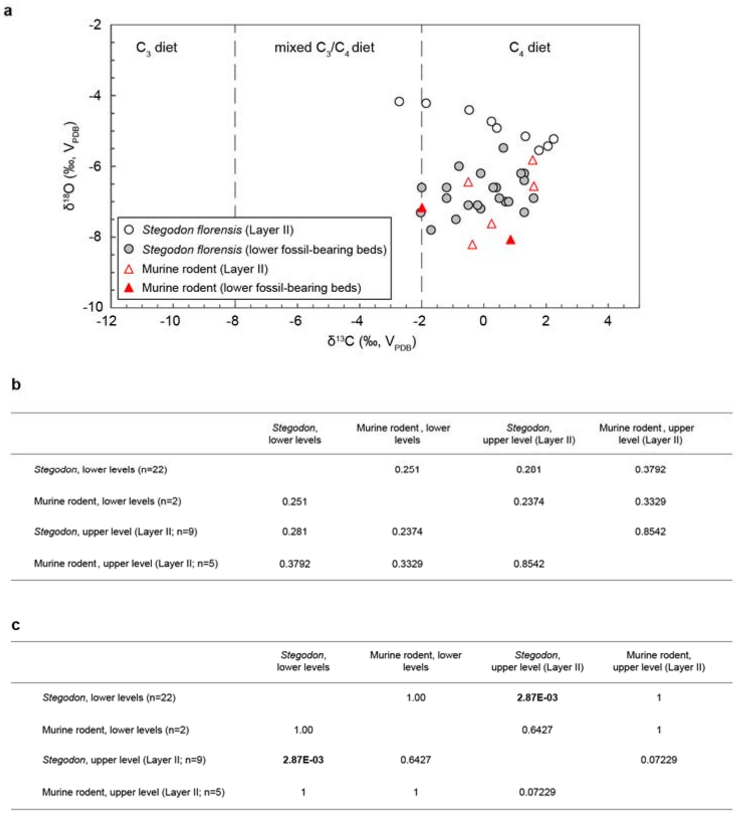

b

	Stegodon, lower levels	Murine rodent , lower levels	*Stegodon*, upper level (Layer II)	Murine rodent , upper level (Layer II)
Stegodon, lower levels (n=22)		0.251	0.281	0.3792
Murine rodent, lower levels (n=2)	0.251		0.2374	0.3329
Stegodon, upper level (Layer II; n=9)	0.281	0.2374		0.8542
Murine rodent , upper level (Layer II; n=5)	0.3792	0.3329	0.8542	

c

	Stegodon, lower levels	Murine rodent, lower levels	*Stegodon*, upper level (Layer II)	Murine rodent, upper level (Layer II)
Stegodon, lower levels (n=22)		1.00	**2.87E-03**	1
Murine rodent, lower levels (n=2)	1.00		0.6427	1
Stegodon, upper level (Layer II; n=9)	**2.87E-03**	0.6427		0.07229
Murine rodent, upper level (Layer II; n=5)	1	1	0.07229	

Extended Data Figure 8. Carbon and oxygen isotope analysis of dental enamel. a, $\delta^{13}C$ and $\delta^{18}O$ values of *Stegodon florensis* and murine rodent tooth enamel. All but one of the $\delta^{13}C$ ratios corresponds with a C_4 diet, indicating that both *Stegodon* and murine rodents were predominantly grazers in both fossil-bearing horizons. The positive shift observed in $\delta^{18}O$ of the younger *Stegodon* samples (from the hominin-bearing Layer II) is more difficult to interpret with the limited data available, but could mean a distinct source of drinking water (run-off versus lacustrine) and/or warmer conditions; **b**, Benferroni corrected p values for a pairwise Mann-Whitney statistical analysis to test for similarity of $\delta^{13}C$ between subsamples; **c**, Benferroni corrected p values for a pairwise Mann-Whitney statistical analysis to test for similarity of $\delta^{18}O$ between subsamples; p values showing significant differences in median values are in bold.

a

Trench	Layer	Assayed cobble	Flake	Multi -platform core	Bifacial core	Modified flake	Total
E-32A	I	1	9	-	-	-	10
	II	1	24	-	-	2	27
	III	-	5	-	-	-	5
	not determined	-	1	-	-	-	1
E-32B	I	-	34	2	1	2	39
	II	-	2	-	-	-	2
	III	-	2	-	-	-	2
	not determined	-	4	-	1	-	5
E-32C	I	-	7	-	-	-	7
	II	-	16	-	1	-	17
	III	-	1	-	-	-	1
	I, II interface	-	9	-	-	1	10
	not determined	-	3	-	-	-	3
E-32D	I	-	3	-	-	-	3
	II	-	1	-	-	-	1
	III	-	1	-	-	-	1
	II, III interface	-	2	-	1	-	3
	not determined	-	4	-	-	1	5
E-32E	I	-	2	-	-	-	2
	III	-	1	-	-	-	1
	not determined	-	2	-	-	-	2
E-32F	not determined	-	2	-	-	-	2
Total		2	135	2	4	6	149

b

Artefact type	Coarse- and medium-grained volcanics	Fine-grained volcanics and silicates	Total
Assayed cobble	2	–	2
Flake	90	45	135
Multiplatform core	1	1	2
Radial core	2	2	4
Retouched flake	2	4	6
Total	97	52	149

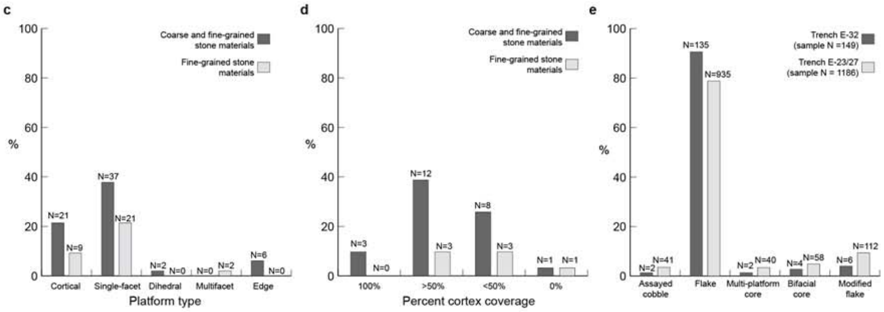

f

Artefact Type	Trench	Metrical summary		
		Largest linear dimension of complete artefacts (mm) (Mean ± SD, sample size)	Grams of complete artefacts (Mean ± SD, sample size)	Largest linear dimension of flake scars on cores and modified flakes (mm) (Mean ± SD, sample size)
Core	E-32	56.4 ± 31.9 (N=8)	189.9 ± 256.9 (N=8)	20.3 ± 12.8 (N=83)
	E-23/27	66.4 ± 27.4 (N=102)	294.1 ± 346 (N=102)	21.3 ± 13.5 (N=1116)
Flake	E-32	33.7 ± 13.5 (N=68)	15.6 ± 21.1 (N=70)	–
	E-23/27	41 ± 16.6 (N=450)	24.5 ± 28.7 (N=451)	–
Modified flake	E-32	34.9 ± 14.5 (N=6)	17 ± 24.8 (N=6)	–
	E-23/27	44.9 ± 16 (N=74)	39.1 ± 73.4 (N=74)	–

g

Trench	Coarse- and medium-grained volcanics	Fine-grained volcanics and silicates
	No, %	No, %
E-32	97 (65.1%)	52 (34.9%)
E-23/27	1025 (86.6%)	158 (13.4%)

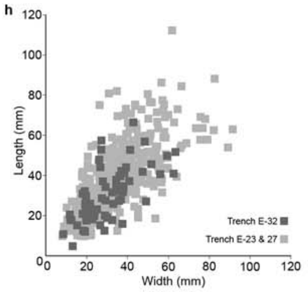

Extended Data Figure 9: Analytical data for the Mata Menge stone technology. **a**, Artefact counts and provenance, Trench E-32 (artefact definitions after ref. 37); **b**, raw materials used to manufacture the stone tool assemblage, Trench E-32; **c**, Platform types on flakes and modified flakes, E-32. Cortical: the blow was struck onto the cortical surface of a cobble. Single-facet: the blow was struck on a scar produced by previous reduction. Dihedral: the blow was struck on the ridge between two scars produced by previous reduction. Multifacet: the blow was struck on the surface of multiple small scars produced by previous reduction. Edge: the blow was struck on the edge of the core and a platform surface is not retained on the flake; **d**, Cortex coverage on the dorsal surface of complete unmodified flakes, E-32. Percent cortex coverage refers to the proportion of the dorsal surface covered in cortex; **e**, Artefact counts, Trenches E-32 and E-23/27 (artefact definitions after ref. 37); **f**, Sizes of artefacts and attributes, E-32 and E-23/27; **g**, Raw materials used to manufacture the stone tool assemblage, E-32 and E-23/27; **h**, Scatterplot of complete flake sizes, E-32 (total sample size [N] = 68 complete flakes) and E-23/27 (N=443). With regards to raw materials, coarse- and medium-grained materials include andesite, basalt, rhyolite, and tuff. Fine-grained materials include silicified tuff, chalcedony, and opal.


Elev (m asl)
405
400
395
390
385
380
375
370
365
360
355
KEY
Stone artefacts
Vertebrate fossils
Hominin fossils
Fossil plant material
Fossil gastropoda
E Excavation (i.e., trench)
P Paleosol
T Tephra
M Mud-flow/debris flow
F Fluviatile clastics
G Gero Member
Erosional contact
E-35
(~600 m W of T12)
G
0.51 ± 0.03 Ma (^{40}Ar/^{39}Ar)
T6
E-12/32
T (PGT-2) 0.65 ± 0.02 Ma (^{40}Ar/^{39}Ar)
E-12
T-UMM
E-37
E-32
Multiple cohesive mass-flow deposits (mudflows) with intervening fluviatile lenses
Layers Ia-f
F (Layer II)
>0.55 Ma
(U-series)
0.36-0.69 Ma
(U-series/ESR)
F (Layer III)
T-LMM
d
E-9/10
T/F (reworked)
T-LMM
0.80 ± 0.07 Ma
(ZFT)
0.88 ± 0.07 Ma
(ZFT)
E-34/34B
T-Pu
0.81 ± 0.04 Ma
(^{40}Ar/^{39}Ar)
T3 (airfall tephra bed)
0.90 ± 0.07 Ma
(ITPFT)
T-T
T-WSI (ignimbrite)
1.01 ± 0.02 Ma
(^{40}Ar/^{39}Ar)
T-W
Ola Kile Fm.
(>1.86 Ma)
Borneo
Sunda
Sulawesi
Flores
See b
Timor
Java
Sahul
0
1000 km
a
Land at present
Emerged land during the Last Glacial Maximum (~22-19 Kyr)
0
20 km
So'a Basin
See c
b
Welas caldera
Lowo Lele
Ae Sissa
Ae Bha
SO'A
MENGERUDA
BAJAWA
N
0
8 km
1800 m
0 m
Sites
Mata Menge
Lowo Mali
Pu Maso
Dozu Dhalu
Tangi Talo
Kobatuwa
Wolo Sege
Boa Lesa
Other locality
c
SOA-MM1
SOA-MM2
SOA-MM4
SOA-MM5
SOA-MM6
Layer II
e
Topsoil
I-a
I-b
III
II
I-c
I-e
I-f
I-d
32D
32E
32C
32B
32A
0 m
1
2
4 5 6 7 8 9 10 11 12 13 14 15 16 17 18 19 20 21 22 23 24 25
K J I H G L M N O P Q R
36
37
12
32
11, 21
26
10
24
28-30
27
19
31D
9
18
1-8
25
23
14-15, 22
29, 31
34/34B
16-17, 20
33
Elev (m asl)
380 370 360 350 340 330
North
400 m
200 m
0 m
Ola Bula Fm.
Ola Kila Fm.
f


a
b
c
d
e
f
g
h
i
j
k